Homeostatic cytokines reciprocally modulate the emergence of prenatal effector PLZF+CD4+ T cells in humans

Veronica Locher[1,2,7], Sara Park[1,2], Daniel Bunis[3,4], Stephanie Makredes[1,2], Trevor D. Burt[5], Gabriela K. Fragiadakis[3,4,6], Joanna Halkias[1,2,3 *]

1. Division of Neonatology, Department of Pediatrics, UCSF, San Francisco, CA, USA, **2.** Eli and Edythe Broad Center of Regeneration Medicine and Stem Cell Research, UCSF, San Francisco, CA, USA, **3.** Bakar ImmunoX Initiative, UCSF, San Francisco, CA, USA, **4**. CoLabs, UCSF, San Francisco, CA, USA, **5**. Division of Neonatology and the Children's Health & Discovery Initiative, Department of Pediatrics, Duke University School of Medicine, Durham, NC, USA**, **6.** Department of Medicine, Division of Rheumatology, UCSF, San Francisco, CA, United States**, 7.** Committee on Immunology, University of Chicago, Chicago, IL, USA**

* Corresponding author

** Current institution

Address correspondence to:

Joanna Halkias, Division of Neonatology, Department of Pediatrics, and Eli and Edythe Broad Center of Regeneration Medicine and Stem Cell Research, UCSF, San Francisco, CA, USA.

Email: joanna.halkias@ucsf.edu

The authors have declared that no conflict of interest exists.

Abstract

The development of human adaptive immunity progresses faster than previously appreciated, with the emergence of memory $CD4^+$ T cells alongside regulatory T (Treg) cells by the second trimester of pregnancy. We previously identified a prenatal-specific subset of $PLZF^+$ $CD4^+$ T cells with heightened effector potential that accounted for most memory T cells in the developing intestine and accumulated in the cord blood of infants exposed to prenatal inflammatory pathologies. However, the signals that drive their tissue distribution and effector maturation are unknown. In this report, we define the transcriptional and functional heterogeneity of prenatal $PLZF^+$ $CD4^+$ T cells and identify compartmentalization of Th-like effector function across the small intestine (SI) and mesenteric lymph nodes (MLN). We find that IL-7, which is more abundant in the SI relative to the MLN, drives the preferential expansion of naïve $PLZF^+$ $CD4^+$ T cells via JAK/STAT and MEK/ERK signaling. Exposure to IL-7 induces a subset of $PLZF^+$ $CD4^+$ T cells to acquire a memory-phenotype and rapid effector function, identifying the human analogue of memory-phenotype $CD4^+$ T cells. Further, IL-7 modulates the differentiation of Th1- and Th17-like $PLZF^+$ $CD4^+$ T cells, and thus likely contributes to the anatomic compartmentalization of prenatal $CD4^+$ T cell effector function.

Introduction

Pregnancy is a critical period of early human immune development. Unlike mice, humans are born with a complete set of immune cells, and T cells are evident in the periphery by 12-14 weeks of gestation. Specifically, αβ and γδ T cells emerge simultaneously during prenatal thymopoiesis, and along with regulatory T (Treg) cells, are evident at mucosal surfaces by the second trimester of pregnancy (1–4). Thus, in humans, the critical early life window of development in which the immune system is highly receptive to environmental instruction (5), begins *in utero*.

Growing evidence supports the notion that prenatal T cells are a specialized population adapted to the unique demands of the perinatal period (6). These include the need for tolerance

53 to self and maternal antigens *in utero* and a simultaneous requirement for the generation of a
54 protective immune compartment to face the multitude of environmental antigens encountered
55 after birth. Thus, the survival of a healthy newborn requires the concurrent generation of both
56 regulatory and protective T cells, adding a layer of complexity to the development of human
57 adaptive immunity.

58 The priming and differentiation of naïve T cells upon encounter with cognate antigen in
59 the context of MHC, co-stimulatory signals, and specific cytokine milieux results in the
60 generation of distinct T helper (Th) cell subsets with characteristic transcriptional and cytokine
61 production profiles (7). In addition to foreign-antigen specific memory Th cells, murine studies
62 have identified memory-phenotype $CD4^+$ T cells which arise in response to interactions with self-
63 peptide MHC in combination with homeostatic cytokines in the setting of lymphopenia-induced
64 proliferation (8,9). A recent study identified that early life $CD8^+$ T cells have a cell-intrinsic
65 propensity to become virtual-memory cells and constitute the early effector response to infection
66 in adulthood (10). Thus, the human *in utero* environment with limited yet impending exposure to
67 a multitude of foreign antigens after birth, and a peripheral compartment largely void of immune
68 cells, is ideally positioned for the generation of memory-phenotype cells to provide rapid
69 protection at mucosal surfaces. However, whether these cells are present in humans is not
70 clear.

71 The majority of T cells in mice and humans alike reside in lymphoid and mucosal
72 tissues, with a heterogeneous distribution of subsets and function across specific sites (11,12).
73 In the mature immune system, the anatomic location of T cells is critical to their differentiation
74 and function. It is likely that the developing prenatal immune system similarly integrates local
75 cues to induce the differentiation of cell types tailored to meet the needs of the tissue they
76 reside in. Naïve T cells predominate in most infant and pediatric tissues, yet memory-phenotype
77 $CD4^+$ T cells with rapid effector function are evident in the SI by the second trimester of
78 pregnancy (13–16). We recently demonstrated that the majority of these intestinal memory T

79 cells express the transcription factor promyelocytic leukemia zinc finger (PLZF), and though
80 present in lymphoid and non-lymphoid tissues, prenatal PLZF$^+$ CD4$^+$ T cells specifically
81 accumulated in the intestine and were superior producers of Th1 cytokines as compared to
82 PLZF$^-$ CD4$^+$ T cells (14). Moreover, PLZF$^+$ CD4$^+$ T cells were enriched in the cord blood of
83 infants exposed to prenatal inflammatory pathologies, underscoring the clinical relevance of
84 understanding the signals that drive the maturation and compartmentalization of these effector T
85 cells *in utero*.

86 To better understand how the prenatal environment shapes the developing human CD4$^+$
87 T cell compartment, we set out to identify the cues that drive T cell maturation and function
88 during normal development. We provide evidence of the functional heterogeneity and spatial
89 segregation of memory PLZF$^+$ CD4$^+$ T cells between the lamina propria of the SI and the
90 draining MLN, revealing a diversity of Th-like effector function that parallels that of conventional
91 CD4$^+$ T cells. We further define tissue-specific differences in homeostatic cytokines and identify
92 IL-7 as a critical driver in the distribution and functional maturation of prenatal effector PLZF$^+$
93 CD4$^+$ T cells, including the generation of memory-phenotype CD4$^+$ T cells in response to
94 lymphopenia-induced proliferation.

95

96 **Results**

97

98 **Prenatal PLZF$^+$ CD4$^+$ T cells are functionally heterogeneous and display spatially**
99 **compartmentalized effector function.**

100 We previously demonstrated that PLZF$^+$ CD4$^+$ T cells account for the majority of memory
101 T cells in the developing human SI (14). Moreover, PLZF$^+$ CD4$^+$ T cells were significantly more
102 likely to produce Th1 cytokines (IFNγ, TNFα) than conventional memory CD4$^+$ T cells,
103 displaying a heightened effector potential and a transcriptional signature enriched for T cell
104 activation genes. To determine their range of effector function, we sort-purified intestinal PLZF$^+$

105 CD4$^+$ T cells as previously described (14) and analyzed their transcriptional response to
106 PMA/Ionomycin stimulation. In addition to Th1-associated transcripts such as *TNF*, *IFNG*, and
107 *XCL2*, stimulated PLZF$^+$ CD4$^+$ T cells also up-regulated transcription of a multitude of cytokines
108 not classically produced by a single T cell subset. These included *IL4* and *IL13*, as well as *IL22*
109 and *LIF* (Figure 1A), suggesting a potentially heterogeneous T cell population composed of
110 distinct effector subsets. To further characterize these effector subsets, we performed single cell
111 RNA sequencing on sort purified PLZF$^+$ CD4$^+$ T cell from 3 individual donors. Unbiased
112 clustering analysis divided 23,676 cells into 7 subsets represented in each donor and annotated
113 by distinct expression signatures (Figure 1B-E; Supplemental Figure 1A). A subset of Th1-like
114 cells with high expression of *XCL1*, *XCL2*, *CCL5*, *IFNG*, and *CXCR3*, as well as activation
115 (*CD38*, *CD44*, *4-1BB/TNFRSF9* and *NR4A2*) and cytotoxicity (*GZMA*, *GZMK*, and
116 *NCR3/NKp30*) markers was readily identified. In line with a Th1-like profile, pathway analysis
117 revealed enrichment of IL-12 signaling, T cell receptor (TCR) signaling, and Natural Killer cell
118 mediated cytotoxicity (Figure 1E and F). Transcripts associated with Th17 cells (*CCR6*, *RORC*,
119 *RORA*, *MAF*, and *IL23R*) marked a second subset with increased expression of IL-2, as well as
120 pathway enrichment for both IL-12 and TGFβ signaling. A Th2-like cluster of PLZF$^+$ CD4$^+$ T cells
121 was characterized by the lineage defining transcription factor *GATA3* and increased expression
122 of *IL32*, *IL16*, and *MIF*, as well as the TCR signaling regulators *CD5* and *CD6*. Proliferating cells
123 were identified based on higher expression of transcripts related to G1/S phase (*CDC45*, *PCNA*,
124 *TYMS*) or G2M phase (*CDK1*, *TOP2A*) (17), consistent with our previous identification of a large
125 proportion of proliferating memory T cells in the prenatal intestine (14). An interferon-stimulated
126 gene (ISG) signature defined another subset of PLZF$^+$ CD4$^+$ T cells, which included the higher
127 expression of *DDX58*, *OAS1*, *MX1*, *IFIT1*, *RSAD2*, and *ISG15*, and was specifically enriched for
128 Type I and Type II Interferon signaling. The ISG signature has been proposed to represent an
129 intermediate Th1 activation state (18) and has also been associated with bystander activation of
130 T cells (19), a defining feature of prenatal PLZF$^+$ CD4$^+$ T cells. Interestingly, cytokine signaling,

131 T cell activation, and T cell differentiation pathways were enriched among most subsets,
132 whereas TCR signaling was uniquely enriched in Th1-like cells. In stark contrast, Cluster 0
133 harbored only 22 differentially upregulated genes and was void of cytokine- and TCR- signaling
134 pathways and markers of lymphocyte activation and differentiation (Figure 1D-F), suggestive of
135 a resting or precursor cell state. Cluster 5, while lacking a distinct gene signature, displayed
136 transcriptional overlap with that of the Th-17 like subset, suggestive of an intermediate or
137 transitional state (Figure 1D and E). Lastly, expression of *TNF* and *LIF* transcripts was evident
138 across all PLZF$^+$ CD4$^+$ T cells without differential expression between subsets (Figure 1G).
139 These distinct transcriptional signatures suggest the presence of different effector branches of
140 prenatal PLZF$^+$ T cells that parallel conventional T helper subsets.

141 We next sought to confirm cytokine production from our predicted Th-like PLZF$^+$ CD4 T
142 cell subsets. We previously showed that PLZF$^+$ CD4$^+$ T cells responded to both TCR activation
143 and to bystander activation in response to cytokines. A role for antigen-independent activation
144 of CD8$^+$ T cells has been described in the setting of inflammatory and/or infectious pathologies,
145 yet less is known about bystander activation of human CD4$^+$ T cells (20–22). To assess the
146 prenatal Th-like effector program, we stimulated intestinal memory CD4$^+$ T cells, with
147 αCD3/CD28 monoclonal antibodies and/or a combination of cytokines known to elicit specific
148 Th-type bystander responses (23). Consistent with our previous findings (14), we observed
149 significantly higher frequencies of IFNγ-producing cells in response to bystander activation
150 among PLZF$^+$ CD4$^+$ CD45RO$^+$ T cells compared to their conventional (i.e., PLZF$^-$ CD4$^+$)
151 counterparts. Differences in IFNγ-production were also evident by anatomic compartment, with
152 significantly higher proportions of both CD4$^+$ memory T cells producing IFNγ in the SI as
153 compared to the MLN, whereas no differences were evident for TNFα (Figure 2A and B,
154 Supplemental Figure 2A). The proportion of IL-13 producing cells in the MLN was higher among
155 PLZF$^+$ than PLZF$^-$ CD4$^+$ CD45RO$^+$ T cells, whereas production of IL-4 was similar (Figure 2C-

156 E). Moreover, IL-4 production was mostly absent from the SI, suggesting Th2-like cells in the
157 developing intestine are primarily IL-13 producing cells with minimal capacity for IL-4 production.
158 Despite the presence of RORγt$^+$ PLZF$^+$ CD4$^+$ T cells in both the MLN and the SI (Supplemental
159 Figure 2B), IL-17 producing cells revealed the most striking segregation of effector function.
160 While the proportion of IL-17 producing cells was similar among memory CD4$^+$ T cells in the
161 MLN across activation conditions, these were essentially absent from the SI (Figure 2F and H).
162 On the other hand, production of IL-22 was significantly higher among memory CD4$^+$ T cells of
163 the SI as compared to the MLN and was elicited almost exclusively in response to bystander
164 activation. Further, IL-22 producing cells were significantly more abundant among PLZF$^+$ than
165 conventional CD4$^+$ memory T cells in the MLN (Figure 2G and H). These findings confirm the
166 presence of functional, cytokine-producing populations that correlate to populations predicted by
167 the transcriptional programs of distinct Th1-, Th2-, Th17-, and Th22-like populations of prenatal
168 PLZF$^+$ CD4$^+$ T cells and reveal a clear pattern of segregation of effector function between the
169 developing human MLN and SI.
170

171 **IL-7 and TGFβ reciprocally regulate the expansion of prenatal naïve PLZF$^+$ CD4$^+$ T cells**

172 Based on the intestinal accumulation of PLZF$^+$ CD4$^+$ T cells (14) and their enrichment for
173 cytokine signaling pathways (Figure 1F), we hypothesized that differences in cytokine levels
174 within tissues might contribute to their disparate distribution. While systemic levels of IL-7 are
175 elevated in the setting of lymphopenia (24), there are significantly higher levels of IL-7 and IL-15
176 in the prenatal SI as compared to the MLN, while IL-2 was largely undetectable (Figure 3A and
177 Supplemental Figure 3). To examine the influence of these cytokines on naïve CD4$^+$ T cells, we
178 opted to study the differentiation of prenatal mature CD4$^+$ TCR$\alpha\beta^+$ CD1α^- single positive
179 thymocytes to exclude prior exposure to peripheral homeostatic signals. There was a significant
180 accumulation of PLZF$^+$ CD4$^+$ T cells in response to IL-7 stimulation in comparison to pre-

181 stimulation (d0) frequencies, an effect that was not evident in the presence of IL-2 or IL-15
182 (Figure 3B and C). We previously demonstrated that naïve PLZF$^+$ CD4$^+$ T cells have a 3-fold
183 higher rate of proliferation as compared to their conventional counterparts (14), and here we
184 show that the accumulation in response to IL-7 was driven by the enhanced proliferation of
185 PLZF$^+$- relative to that of PLZF$^-$ naïve CD4$^+$ T cells in a dose-dependent manner (Figure 3D and
186 E).

187 Murine studies identify a correlation between surface expression of CD5, a marker of
188 TCR signal strength on naïve CD4$^+$ and CD8$^+$ T cells, and the intensity of lymphopenia-induced
189 proliferation (25,26). We demonstrate here that naive PLZF$^+$ CD4$^+$ T cells expressed higher
190 levels of CD5 as compared to their PLZF$^-$ counterparts (Figure 3F and G), suggesting that the
191 enhanced response to IL-7 was set during thymic selection (27). To confirm that the effects of
192 IL-7 were due to the expansion of a thymus-derived PLZF$^+$ CD4$^+$ T population, we sorted on
193 proxy surface markers to enrich and deplete the native population of naïve PLZF$^+$ cells
194 (Supplemental Figure 4). This sorting strategy yielded significant differences in the proportion of
195 PLZF$^+$ CD4$^+$ T cells within the enriched vs depleted fractions which were maintained after 6
196 days of culture in IL-7 (Figure 3H and I). These data indicate that the accumulation of PLZF$^+$
197 CD4$^+$ T cells in response to IL-7 is driven by the enhanced proliferation of a pre-existing
198 population of PLZF$^+$ CD4$^+$ thymocytes.

199 While intestinal accumulation of PLZF$^+$ CD4$^+$ T cells is associated with higher tissue
200 levels of IL-7, reported frequencies of FoxP3$^+$ Treg cells are reciprocally increased in the
201 prenatal MLN (13,28) and correlate with elevated levels of TGFβ that contributes to their
202 generation (29). We thus postulated that TGFβ would inhibit the accumulation of PLZF$^+$ CD4$^+$ T
203 cells. Indeed, we found that TGFβ significantly dampened the accumulation of PLZF$^+$ CD4$^+$ T
204 cells in response to IL-7 by specifically inhibiting their proliferation relative to their
205 PLZF$^-$ counterparts (Figure 3J-M). These data provide evidence that variation in steady state

206 cytokine levels likely contributes to the disparate distribution of PLZF$^+$ CD4$^+$ T cells in prenatal
207 tissues.
208
209 **Differences in IL7 signaling contribute to the preferential expansion of PLZF$^+$ CD4$^+$ T cells**
210 IL-7 is known to drive the homeostatic expansion of human naïve CD4$^+$ T cells during
211 early life lymphopenia (30), which led us to determine the basis for the expansion of naïve
212 PLZF$^+$ CD4$^+$ T cells relative to their PLZF$^-$ counterparts. The interaction between IL-7 and the IL-
213 7 receptor (IL-7R/CD127) activates JAK1 and JAK3/STAT5 signaling as well as STAT5-
214 independent signal transduction pathways including PI3K/AKT and MEK/ERK (31). Expression
215 of IL-7R was significantly more prevalent among PLZF$^+$ CD4$^+$ T cells, whereas expression of the
216 receptors for IL-2 and IL-15 did not differ from those of their PLZF$^-$ counterparts (Figure 4A and
217 B and Supplemental Figure 5A-F). Consistent with the pattern of cytokine receptor expression,
218 STAT5B phosphorylation (i.e., pSTAT5B) was induced at higher levels in paired naïve PLZF$^+$ as
219 compared to PLZF$^-$ CD4$^+$ T cells in response to IL-7, but not in response to IL-2 or IL-15 (Figure
220 4C-D, Supplemental Figure 5G-H). To assess the contribution of STAT5-dependent and -
221 independent signaling in the IL-7 driven expansion of human prenatal PLZF$^+$ CD4$^+$ T cells, we
222 treated naïve CD4$^+$ T cells exposed to IL-7 with a range of signaling inhibitors *in vitro.* As
223 expected, the accumulation of PLZF$^+$ CD4$^+$ T cells in response to IL-7 was almost entirely
224 dependent on JAK1 and JAK3 signaling. A similar dependency on STAT5 and STAT3 was also
225 evident in response to the combined inhibitor SH-4-54 and was surprisingly replicated by the
226 STAT3-specific small molecule inhibitor STAT3-in-1. We additionally observed significant PLZF$^+$
227 CD4$^+$ T cell sensitivity to the selective PI3K inhibitor GDC-0941/Pictilisib and the MEK/ERK
228 pathway inhibitor PD0325901 (Figure 4E). While all signaling inhibitors dampened expansion of
229 PLZF$^+$ CD4$^+$ T cells, these cells displayed selective inhibition to MEK/ERK signaling which had
230 no discernable effect on their PLZF$^-$ counterparts (Figure 4F and G). In addition, there was also
231 a significantly greater effect on the expansion of PLZF$^+$ compared to PLZF$^-$ CD4$^+$ T cells in

232 response to the combined STAT3/5 inhibitor. In sum, the increased frequency of IL7R
233 expression among PLZF$^+$ CD4$^+$ T cells correlates with higher levels of STAT5B phosphorylation,
234 and there is a selective sensitivity to MEK/ERK signaling in PLZF$^+$ CD4$^+$ T cells which may
235 additionally contribute to their enhanced proliferation in response to IL-7.
236
237 **Prenatal PLZF$^+$ CD4$^+$ T cells are MHC II-restricted and TCR signaling does not interfere**
238 **with IL-7 driven expansion**
239 IL-7 can function independently of, or synergize with, TCR signaling to promote
240 proliferation of naïve CD4$^+$ T cells (32). As prenatal PLZF$^+$ CD4$^+$ T cells share functional and
241 transcriptional attributes with both conventional and innate-like T cells (14), we next sought to
242 determine whether PLZF$^+$ CD4$^+$ T cell activation was mediated by recognition of MHC II. We
243 therefore examined the activation of SI memory PLZF$^+$ CD4$^+$ T cells in the presence or absence
244 of a blocking antibody for MHC class II-TCR interactions during short-term exposure to
245 allogeneic adult CD14$^+$ antigen presenting cells *ex vivo*. To quantify the allogeneic response, we
246 calculated the stimulation index, defined as the proportion of the PLZF$^+$ CD4$^+$ T cells that
247 upregulated expression of the activation molecule CD154 multiplied by the proportion of IFNγ-
248 producing cells (33). We found that the stimulation index of PLZF$^+$ CD4$^+$ T cells was significantly
249 reduced in the presence of a pan-MHC class II blocking antibody in comparison to isotype
250 control (Figure 5A and B). Thus, consistent with expression of a polyclonal TCR repertoire (14),
251 prenatal PLZF$^+$ CD4$^+$ T cells recognized antigen in the context of MHC class II, suggesting a
252 stronger similarity to conventional CD4$^+$ T cells than to innate-like T cells.

253 We next evaluated the influence of TCR activation on the expansion of PLZF$^+$ CD4$^+$ T
254 cells in response to IL-7. TCR activation via αCD3/CD28 cross-linking did not affect their
255 preferential accumulation in the presence of IL-7 as compared to IL-2 (Fig. 5C, D), and this was
256 consistent across varying levels of αCD3 stimulation (Fig. 5E). We excluded the possibility that

257 low-level TCR signaling from T cell-T cell interactions (34) might contribute to the IL-7 driven
258 accumulation of PLZF$^+$ CD4$^+$ T cells as this was unchanged in the presence of a pan-MHC class
259 II blocking antibody (Supplemental Figure 6A and B). Further, TCR engagement had no effect
260 on the ability of TGFβ to inhibit the IL-7 driven accumulation and proliferation of PLZF$^+$ CD4$^+$ T
261 cells (Fig. 5F-I). As prenatal naïve T cells are known to preferentially generate Treg cells we
262 also examined the effect of IL-7 on the differentiation of these (29). Whether naïve CD4$^+$ T cells
263 were activated in the absence of Th skewing conditions (Th0; IL-2 alone) or under Treg skewing
264 conditions (IL-2 + TGFβ), addition of IL-7 significantly inhibited the generation of Treg cells (Fig.
265 5J-M). These data indicate that IL-7 and TGFβ may conversely contribute to the tissue-specific
266 accumulation of PLZF$^+$ CD4$^+$ T cells and Treg cells.
267
268 **Prenatal PLZF$^+$ CD4$^+$ T cells acquire a memory-phenotype independent of TCR signaling**
269 As long-term polyclonal stimulation of human naïve T cells *in vitro* results in the
270 generation of CD45RO$^+$ memory cells (35), we next analyzed induction of a memory phenotype
271 in PLZF$^+$ CD4$^+$ T cells exposed to IL-7 in the presence of varying levels of αCD3/CD28
272 stimulation. A small proportion of CD45RO$^+$ cells emerged at higher levels of prolonged
273 polyclonal stimulation among conventional CD4$^+$ T cells, and the frequencies of memory-
274 phenotype cells were significantly higher among PLZF$^+$ CD4$^+$ T cells across all conditions
275 (Figure 6A and B). Moreover, expression of CD45RO was induced among PLZF$^+$ T cells
276 exposed to IL-7 alone and was unaffected by blockade of MHC-TCR interactions (Figure 6B,
277 Supplemental Figure 7A). To determine whether expression of CD45RO corresponded with the
278 potential for cytokine production, we next stimulated CD4$^+$ T cells with PMA/Ionomycin after 12
279 days of culture in the presence of IL-7 and increasing levels of TCR activation. While the
280 potential for TNFα production was high among all subsets of prenatal CD4$^+$ T cells, the
281 proportion of TNFα^+ cells was consistently higher in PLZF$^+$ as compared to PLZF$^-$ CD4$^+$ T cells

282 and did not differ across levels of αCD3 activation (Figure 6C and D). Conversely, IFNγ
283 production was nearly absent from PLZF$^-$ CD4$^+$ T cells, while the proportion of IFNγ$^+$ PLZF$^+$ T
284 cells was inversely related to the dose of αCD3 stimulation (Figure 6C and E). These data
285 indicate that a subset of prenatal PLZF$^+$ CD4$^+$ T cells acquire a memory-like phenotype and
286 potential for IFNγ production in the absence of TCR stimulation, akin to memory-phenotype
287 murine CD4$^+$ T cells.

288 **IL-7 modulates effector function of prenatal PLZF$^+$ CD4$^+$ T cells**

289 We next asked whether memory-like PLZF$^+$ CD4$^+$ T cells generated in response to IL-7
290 alone, or in combination with TCR signaling, could produce cytokines in response to antigen
291 receptor-mediated or bystander activation. To ensure sufficient cell numbers for functional
292 interrogation, we first cultured naïve CD4$^+$ T cells in IL-7 for 6 days to promote expansion of
293 PLZF$^+$ CD4$^+$ T cells and subsequently differentiated them in the presence of αCD3/CD28 and
294 various combinations of cytokines (Supplemental Figure 8A). A subset of PLZF$^+$ CD4$^+$ T cells
295 produced IFNγ in response to both TCR- and cytokine-mediated activation after prolonged
296 culture in IL-7 alone, as well as TNFα in response to TCR activation, while cytokine production
297 was mostly absent from PLZF$^-$ CD4$^+$ T cells (Figure 7A, Supplemental Figure 8B). Interestingly,
298 differentiation of naïve CD4$^+$ T cells in the absence of lineage skewing conditions (Th0) did not
299 generate IFNγ-producing cells in response to TCR-mediated activation yet resulted in
300 significantly higher proportions of PLZF$^+$ CD4$^+$ T cells capable of IFNγ production in response to
301 bystander activation as compared to their PLZF$^-$ counterparts (Figure 7B). Moreover, the
302 proportion of bystander-responsive PLZF$^+$ CD4$^+$ T cells was further enhanced by addition of IL-
303 7, whereas TNFα production was unaffected (Figure 7B, Supplemental Figure 8C). Whole
304 tissue levels of IL-12p70, the bioactive form of IL-12 required for Th1 differentiation, were
305 comparable between the SI and the MLN, indicating that low-level, homeostatic production

306 could contribute to the generation of these effector T cells (Supplemental Figure 8D). Though
307 Th1 differentiation induced the generation of TCR-responsive, IFNγ- and TNFα-producing $CD4^+$
308 T cells, the proportion of these was consistently higher among $PLZF^+$ $CD4^+$ T cells. Further,
309 addition of IL-7 to Th1 differentiation conditions specifically enhanced the proportion of IFNγ-
310 producing $PLZF^+$ $CD4^+$ T cells in response to both TCR-mediated and bystander activation yet
311 had no effect on their $PLZF^-$ counterparts (Figure 7C and D, Supplemental Figure 8E).
312 Despite the observed compartmentalization of IL-17 producing $CD4^+$ T cells to the MLN
313 (Figure 2F), tissue levels IL-1β and IL-23 required for human Th17 differentiation were
314 significantly higher in the SI (Supplemental Figure 8F). Naive $CD4^+$ T cells differentiated in the
315 presence of IL-1β and IL-23 induced the capacity for IL-17 production almost entirely within the
316 $PLZF^+$ subset, and the proportion of these was unaffected by addition of IL-6, or IL-6 plus TGFβ
317 (Supplemental Figure 8G). However, addition of IL-7 to Th17 differentiation conditions
318 significantly dampened the potential for IL-17 production among $PLZF^+$ $CD4^+$ T cells (Figure 7E,
319 F). Together, these data reveal a role for IL-7 in modulating effector maturation of prenatal
320 $PLZF^+$ $CD4^+$ T cells, where IL-7 reciprocally enhances production of IFNγ and inhibits the
321 potential for IL-17 production. This divergent maturation in response to IL-7 is likely a
322 contributing factor to the observed compartmentalization of prenatal $CD4^+$ T cell effector
323 function between the prenatal SI and the MLN.
324
325 **Discussion**
326 This study provides evidence of the emergence of human protective adaptive immunity
327 with anatomically compartmentalized effector function during the second trimester of human
328 gestation that parallels conventional Th1, Th2, Th17, and Th22 cells. Through transcriptional
329 analysis, protein validation, and *in-vitro* culture of primary human cells we identified a critical
330 role for IL-7 in the tissue-specific accumulation and effector maturation of human prenatal

331 PLZF$^+$ CD4$^+$ T cells that likely contributes to their intestinal segregation. These results build on
332 the current shift in our understanding of human prenatal immunity from one of functional
333 immaturity to that of a specialized adaptation to meet the demand for prenatal tolerance and
334 concurrently provide rapid postnatal protection.

335 Layering, or progressive transitions in the developmental origin, of CD4$^+$ T cells is
336 thought to underlie the preferential generation of Treg cells upon antigen-mediated activation of
337 prenatal naïve T cells in the periphery (29). Our previous work extended our understanding of
338 prenatal adaptive immunity to include human PLZF$^+$ CD4$^+$ T cells with rapid Th1-like effector
339 function that were absent from the adult (14). Evidence of specialized early life adaptive
340 immunity is well established in mice, in which neonatal CD8$^+$ T cells preferentially develop into
341 virtual-memory T cells with innate immune functions and play a role in the early response to
342 infection (10). Less is known about the origin and function of memory-phenotype CD4$^+$ T cells,
343 which are thought to exist in humans but have been mostly studied in mice.

344 In the setting of physiologic early life lymphopenia, the peripheral T cell pool is driven by
345 thymic output and rapid expansion of naïve T cells in an environment with high levels of
346 homeostatic cytokines (36–38). A central role for IL-7 has been identified in the homeostatic
347 proliferation and survival of murine and human naïve CD4$^+$ T cells (30,39). Moreover,
348 lymphopenia induced proliferation in neonatal mice resulted in the generation of memory
349 phenotype CD4$^+$ T cells with rapid effector function (9). Subsequent studies demonstrated that
350 the rapid proliferation of memory-phenotype CD4$^+$ T cells in young mice was driven by IL-7 (40).
351 Systemic levels of IL-7 are increased in lymphopenic hosts (24), with the highest levels reported
352 in lymphoid organs such as the thymus and lymph nodes (41). It is thus notable that we
353 detected significantly higher levels of IL-7 protein in the human prenatal intestine as compared
354 to the draining lymph nodes, which mirrors the preferential accumulation of memory PLZF$^+$
355 CD4$^+$ T cells with enhanced Th1-like effector function in the intestine. Our data provide evidence
356 for the IL-7 driven proliferation, and the acquisition of memory-phenotype and innate function

357 among a subset of thymic-imprinted, naïve PLZF$^+$ CD4$^+$ T cells, and identify the human
358 analogue of early life memory-phenotype CD4$^+$ T cells.
359 In mice, the generation of memory-phenotype CD4$^+$ T cells is dependent on tonic, low-
360 level signaling from TCR-MHC class II interactions and thought to be driven primarily in
361 response to self-antigens (8). Self-reactivity is evident among human prenatal CD4$^+$ T cells
362 (29), and we and others have also demonstrated that prenatal intestinal CD4$^+$ T cells responded
363 to microbial antigens (42,43). Although blocking TCR-MHC class II interactions in the short term
364 did not influence the proliferation or the acquisition of memory-phenotype of PLZF$^+$ CD4$^+$ T cells
365 *in vitro*, it is possible that TCR signals are required for their long-term survival *in vivo* (44).
366 Future work will determine whether IL-7-expanded and *ex-vivo* isolated prenatal T cells are
367 responsive to self- and/or foreign antigens.
368 T cell activation in response to cognate antigen remains one of the hallmark features of
369 adaptive immunity. In the setting of early life, recognition of danger signals through antigen-
370 independent activation may serve a rapid protective function at barrier surfaces. Similar to
371 virtual memory CD8$^+$ T cells, memory-phenotype CD4$^+$ T cells have been reported to provide
372 early protection against pathogens (8,45), suggesting a vital role in the setting of early life
373 immunity. In stark contrast to the mucosal predominance of Th17 cells in mice (46) and human
374 adults (47), prenatal IL-17 producing CD4$^+$ T cells segregated to the MLN and were absent from
375 the SI, which instead contained higher frequencies of IL-22 producing cells. The anatomic
376 segregation of steady state prenatal IL-17- and IL-22-producing CD4$^+$ T cells to the MLN and SI
377 respectively may serve to limit *in utero* inflammation upon encounter with swallowed luminal
378 antigens or inflammatory mediators while promoting the development and maintenance of
379 epithelial barrier function (48). Production of IL-22 among CD4$^+$ T cells was elicited almost
380 exclusively to bystander activation, which suggests a memory-phenotype origin, and more work
381 is needed to identify the cues that drive their effector maturation.

382 The heterogeneity and spatial segregation of effector function posits that PLZF$^+$ CD4$^+$ T
383 cells are composed of a combination of lymphopenia-induced, memory-phenotype cells as well
384 as antigen-experienced memory T cells. Though PLZF expression is imprinted during thymic
385 development, neither mature CD4 thymocytes nor naïve peripheral CD4 T cells were capable of
386 IFNγ production, indicating that unlike MAIT or NKT cells, additional steps were required for
387 effector maturation (14). We show that PLZF$^+$ CD4$^+$ T cells recognize antigen in the context of
388 MHC class II, which coupled with a polyclonal TCR repertoire (14), indicates significant overlap
389 with conventional CD4$^+$ T cells, including the presence of distinct Th-like subsets. Migratory
390 antigen presenting cells capable of sensing pathogen and stimulating T cells are evident by the
391 second trimester of gestation (49), and antigen-specific immunity to prenatal pathogen exposure
392 is well documented (50), indicating that Th-differentiation is likely occurring *in utero*. We
393 detected low yet consistent levels of Th-skewing cytokines within the prenatal intestine, which
394 consistently elicited a more robust effector response from PLZF$^+$ CD4$^+$ T cells *in vitro*. Moreover,
395 our data identify a role for IL-7 in the modulation of Th1- and Th17-like differentiation among
396 PLZF$^+$ CD4$^+$ T cells and provide a plausible mechanism for the tissue-specific segregation of
397 prenatal effector function.
398 Beyond extending our understanding of human immune ontogeny, an improved
399 understanding of the composition, spatial distribution, and functional responses of prenatal T
400 cells is foundational to the development of early life immunomodulatory interventions with
401 potentially lifelong consequences on immune health.
402
403
404 Methods
405
406 **Cell Isolation**

407 PBMCs from adult blood were isolated by Ficoll-Histopaque (Sigma-Aldrich) gradient
408 centrifugation and cryopreserved in freezing medium (90% FBS + 10% DMSO; ATCC) for batch
409 analysis. Prenatal organs were processed within 2 hours of collection as previously described
410 (14). Briefly, the MLN and SI were dissected, washed, and cut into 1 cm fragments. Mucus from
411 the SI was removed by DTT washes, and the SI epithelial layer was removed by EDTA washes.
412 The MLN and SI were digested in collagenase IV (Life Technologies) and DNase (Roche),
413 filtered, and lymphocytes isolated by 20/40/80 Percoll (GE Healthcare) gradient centrifugation.
414 Intestinal CD4 T cells were isolated by negative selection using the EasySep Human CD4 T Cell
415 Isolation Kit (STEMCELL Technologies). Thymocyte single cell suspensions were obtained by
416 pressing minced tissue though a 70μm strainer. Mature CD4 single positive (SP) thymocytes
417 were negatively enriched using the EasySep Biotin Positive Selection Kit for depletion
418 (STEMCELL Technologies) as previously described (51). Viability was measured with Trypan
419 Blue (Sigma Aldrich).
420
421 **Antibodies and Flow Cytometry**
422 Cells were incubated in 2% FCS in PBS with 1 mM EDTA with human Fc block (STEMCELL
423 Technologies) and stained with Aqua LIVE/DEAD Fixable Dead Cell Stain Kit (Invitrogen) and
424 fluorochrome-conjugated antibodies against surface markers. Intracellular protein and cytokine
425 staining was performed using the Foxp3/Transcription Factor Staining Buffer Set (Tonbo
426 Biosciences). Mouse and rat anti-human monoclonal antibodies (mAbs) used in this study
427 included: IFNγ FITC (clone 25723.11, BD Biosciences, cat# 340449), TCRαβ Percp 710 (clone
428 IP26, Invitrogen, cat# 46-9986-42), TCRγδ Pe-CF594 (clone B1, BD Biosciences, cat# 562511),
429 CD45RA PE-Cy7 (clone HI100, BD Biosciences, cat# 560675), CD4 APC-H7 (clone L200, BD
430 Biosciences, cat# 560837), PLZF APC (clone 6318100, R&D, cat# IC2944A), TCR Va7.2
431 BV605 (clone 3C10, BioLegend, cat# 351720), CD45RO BV650 (clone UCHL1, BioLegend,

432 cat# 304232), TNFα BV711 (clone MAb11, BioLegend, cat# 502940), CD161 BV785 (clone HP-
433 3G10, BioLegend, cat# 339930), CD45 BUV395 (clone HI30, BD Biosciences, cat# 563792),
434 CD3 BUV737 (clone UCHT1, BD Biosciences, cat# 612750), CD8 APC-R700 (clone RPA-T8,
435 BD Biosciences, cat# 565166), IL22 FITC (clone 22URT1, Invitrogen, cat# 11-7229-42), IFNg
436 BV421 (clone 4S.B3, BD Biosciences, cat# 564791), IL2 BV711 (clone 5344.111, BD
437 Biosciences, cat# 563946), IL17A BV421 (clone BL168, BioLegend, cat# 512322), IFNγ BV711
438 (clone 4S.B3, BioLegend, cat# 502539), IL13 PE (clone JES10-5A2, BioLegend, cat# 501903),
439 IL4 BV421 (clone MP4-25D2, BioLegend, cat# 500826), Vα7.2 Biotin (clone 3C10, BioLegend,
440 cat# 351724), Vα2.4 Biotin (clone 6B11, Invitrogen, cat# 13-5806-82), Streptavidin APC-R700
441 (BD Biosciences, cat# 565144), CD154 PE (clone TRAP1, BD Biosciences, cat# 555700),
442 TNFα PECy7 (clone MAb11, BD Biosciences, cat# 557647), CTV BV421 (Thermo Fisher, cat#
443 C34571), IFNγ BV605 (clone 4S.B3, BioLegend, cat# 502536), CD8 BV711 (clone RPA-T8, BD
444 Biosciences, cat# 563677), CD215 BV421 (clone JM7A4, BD Biosciences, cat# 747704),
445 CD127 BV786 (clone HIL-7R-M21, BD Biosciences, cat# 563324), CD25 FITC (clone M-A251,
446 BioLegend, cat# 356106), CD8 FITC (clone RPA-T8, BioLegend, cat# 301050), CD161 BV711
447 (clone DX12, BD Biosciences, cat# 563865), FOXP3 PE (clone PCH101, Invitrogen, cat# 12-
448 4776-41), PD-1 BV605 (clone EH12.2H7, BioLegend, cat# 329924), CD8 PeCY7 (clone RPA-
449 T8, BD Biosciences, cat# 557746), Streptavidin BV605 (BioLegend, cat# 405229), CCR7
450 BV421 (clone G043H7, BioLegend, cat# 353208), CD4 APC-Cy7 (clone RPA-T4, BioLegend,
451 cat# 300517), Aqua LD (Invitrogen, cat# L34957).
452
453 For phosphoflow staining, 1M $CD4^+$ SP thymocytes were stimulated with IL-7 at 5ng/mL for 30
454 minutes at room temperature. The reaction was stopped by adding Fix/Perm and subsequently
455 stained for pSTAT5B (pY694, BD Biosciences) in a 96-well plate using the Foxp3/Transcription
456 Factor Staining Buffer Set. All data were acquired with an LSR/Fortessa Dual SORP flow

457 cytometer (BD Biosciences) and analyzed with FlowJo V10.0.8 (TreeStar) software. Expansion
458 Index was calculated using FlowJo software according to the formula: expansion index= (1-
459 PF)/(1-DiI), where PF=fraction of the original population dividing at leads once during the culture
460 period and DiI=percentage of cells in the final population that have divided.
461
462 **Bulk RNA seq**
463 T cells were isolated as described above from the intestine of 3 individual samples and PLZF$^+$
464 CD4$^+$ TCR-β$^+$ T cells were sorted on proxy surface markers using FACSAria2 SORP (BD
465 Biosciences) as previously described (14). Half the sorted cells were stimulated with 50 ng/ml
466 PMA (Santa Cruz Biotechnology Inc.) and 5μg/ml Ionomycin (Sigma-Aldrich) for 3 hours at 37°C
467 in 4% O2, the remaining cells were left unstimulated. RNA was extracted and purified with the
468 Dynabeads mRNA DIRECT Purification Kit (Thermo Fisher Scientific). mRNA libraries were
469 constructed using the Nugen/Nextera XT Library Prep Kit (Illumina), and 3 samples (3 donors)
470 were sequenced on an Illumina HiSeq 4000 by the Functional Genomics Core Facility at UCSF.
471 The reads from the Illumina HiSeq sequencer in fastq format were verified for quality control
472 using the fastqc software package. Reads were aligned to the human genome (hg38) and read
473 counts aggregated by gene using the Ensembl GRCh38.78 annotation using STAR (52). The
474 transcriptome of unstimulated prenatal PLZF$^+$ CD4$^+$ T cells used for comparison was previously
475 published (14). Differential gene expression analysis was performed on all genes with at least
476 10 reads with the DESeq2, version 1.16.1 (53). Volcano plots were created with ggplot2
477 depicting DE genes (log2 fold change > 0.5, FDR ≤ 0.05).
478
479 **Single Cell RNA-seq**
480 Single, live PLZF$^+$CD4$^+$ TCRαβ$^+$ T cells from the SI were sorted on proxy markers as previously
481 described (14). Post-sort purity was > 87% as determined by intracellular staining for PLZF.

482 Single cells were captured by droplet-based microfluidics, lysed and sequencing libraries
483 prepared in a single bulk reaction following the 10X Genomics protocol,
484 and transcripts were sequenced using a HiSeq4000 System (Illumina). FASTQ files from each
485 multiplexed capture library were mapped to a custom reference containing GRCh19 using the
486 cellranger (v2.0.0) (10X Genomics) count function. After demultiplexing cells into samples,
487 Seurat (v3.1.5) was used to perform quality control filtering of cells. Cells were retained if they a)
488 contained ≥500 reads, b) ≤5% reads coming from mitochondrial genes, and c) called a singlet
489 by Demuxlet, leaving 23,676 cells for downstream analysis. Data was log normalized then
490 principal components analysis was run on variable features selected by the
491 FindVariableFeatures function after scaling with regression of percent mitochondrial and
492 nReads per cell. UMAP and Louvain clustering were performed with Seurat defaults and
493 resolution 0.3. Differential gene expression between subsets of PLZF$^+$ CD4$^+$ T cells was
494 performed using FindAllMarkers with Seurat's MAST implementation (54). Genes were deemed
495 significantly different if an FDR < 0.05, an average fold change > 1.2, and the gene was
496 detected in >5% of cells in either comparison group. Visualizations were created with dittoSeq
497 (v1.6.0) (55). Gene set analyses were performed using Metascape (56) with visualizations
498 created in R with ggplot2.
499
500 **CD4 T cell Stimulation assays**
501 Single cell suspensions of isolated CD4 T cells from the SI and MLN were cultured in a 96-well
502 U-bottom plate in complete RPMI (cRPMI) supplemented with 10% FBS, 10 mM HEPES, 2 mM
503 L-glutamine, and 1X nonessential amino acids and stimulated with plate-bound αCD3 mAb
504 (clone HIT3a, BioLegend, cat#300313) at 1 µg/mL and soluble αCD28 mAb (CD28.2,
505 Invitrogen, cat#MA1-20792) at 2 µg/mL, and/or cells were activated with recombinant human IL-
506 12 and IL-18 (R&D Systems), or IL-2 and IL-33, and/or IL1β and IL-23 for 16–20 hours at 37°C

507 in 4% O2, and Brefeldin A was added for the last 4 hours. All cytokines used at 50ng/mL and
508 from Peprotech unless otherwise specified. After stimulation, cells were stained for intracellular
509 cytokine production as described above. For allogeneic stimulation of prenatal CD4 T cells,
510 adult, unrelated $CD14^+$ cells were isolated from PBMCs with the CD14 Positive Selection Kit II
511 (STEMCELL Technologies), plated in a 96-well plate at a density of 0.5M $CD14^+$ cells/well and
512 allowed to adhere. Non-adherent cells were removed after 30min and adherent cells were
513 incubated with αMHC DP-DQ-DR mAb (BioLegend, clone Tü39) or isotype control (IgG2a,
514 clone MOPC-173, BioLegend) at 10ug/mL for 30 minutes at 37 C. SI $CD4^+$ T cells isolated and
515 enriched as above, and stained with Cell Trace Violet (CTV; Invitrogen) to differentiate these
516 from residual adult T cells and co-cultured at a 4:1 (T:APC) cell ratio for 16 hours, with Brefeldin
517 A added in the last 4 hours. Cells were stained for intracellular CD154, and cytokine production
518 as described above.
519
520 **Naïve CD4 T cell expansion, maturation, and differentiation assays**
521 Mature CD4 single positive (SP) thymocytes were isolated as above and served as the source
522 of naïve CD4 T cells. Cells were cultured with IL-7 (5 ng/mL), IL-2 (10 ng/mL), or IL-15 (10
523 ng/mL) for 7 days with media changes every 2-3 days. Cells were kept at 37C and 4% O_2 for the
524 duration of the stimulation. In some cases, IL-7 doses were titrated as indicated, and/or TGFβ
525 (10ng/mL) was added for the duration of culture. TCR stimulation was provided by plate-bound
526 αCD3 (clone HIT3a, BioLegend, cat#300313) at 1μg/mL unless otherwise specified, and soluble
527 αCD28 (clone CD28.2, BD, cat#555725) at 2μg/mL. For naïve T cell maturation and
528 differentiation assays, cells were washed and moved to a new 96-well plate at day 5-6, rested
529 for 24hrs in the absence of cytokines, and either matured further with IL-7 (5ng/mL) and/or IL-2
530 (10ng/mL) in the presence or absence of TCR stimulation as described above or under Th-
531 skewing conditions for an additional 7 days. Cells were differentiated in the presence of TCR

532 stimulation and IL-2 (10ng/mL) for Th0, with the addition of IL-12 (2.5ng/mL) for Th1, and the
533 addition of IL-1b (10ng/mL) and IL-23 (10ng/mL) for Th17, in the presence or absence of IL-7
534 (5ng/mL). For Th17 differentiation, cells were cultured in IMDM + 10% FBS with 1X non-
535 essential amino acids, 2mM L-glutamine, 10mM HEPES, and Penicillin/Streptomycin. At day 14
536 of culture, cells were washed, replated, and rested for 24 hours as above, and re-stimulated
537 with plate-bound αCD3 (1µg/mL) and soluble αCD28 (2µg/mL) or rhIL-12and rhIL-18 (50ng/mL)
538 for 24 hours. Where indicated, cells were re-stimulated with Phorbol 12-myristate 13-acetate
539 (PMA) and Ionomycin for 4 hours. Brefeldin A was added for the last 4 hours of each
540 stimulation.
541
542 **Chemical Inhibition**
543 Cells were labelled with CTV to track cell proliferation and cultured with IL-7 (10ng/mL) in the
544 presence or absence of chemical inhibitors at 37C in 4%O2 and 5%CO2. Chemical inhibitors
545 from Selleck Chemicals included 5µM SH-4-54 (cat#S7337), 500nM PD0325901 (StemRD,
546 cat#PD-010), 1uM Pictilisib/GDC-0941 (cat#S1065), 5uM Stat3-in-1 (cat#S0818), 50µM JANEX-
547 1 (cat#S5903), and 10µM Solcitinib (cat#S5917). DMSO vehicle control was used at 1µg/mL
548 and 10µg/mL.
549
550 **Protein Extraction and Cytokine Level Quantification from Solid Tissue**
551 Sections of tissue (~10mg) were taken from the SI lamina propria and MLN and placed in chilled
552 Lysis Buffer (1µL/mL Protease inhibitor, 3µL/mL 500mM PMSF in RIPA Buffer). Tissue was
553 disrupted by mixing 20x with a 1mL pipette tip cut to a 2mm opening then vortexed for 15
554 seconds. Tubes were shaken at 4C for 20 minutes at 300rpm and then the entire process was
555 repeated. Tissue was centrifuged at 14,000 rpm for 10 minutes at 4C and supernatant was
556 collected. Tissue IL-7 and IL-15 concentrations were measured via Cytokine Bead Array using

557 the Human Hematopoietic Stem Cell Panel Kit (LEGENDplex). IL-12p70, IL-18, IL-1b, and IL-23
558 concentrations were measured using the Human Inflammation Panel 1 Kit (LEGENDplex).
559
560 **Statistics**
561 Data were analyzed using Wilcoxon's test for paired nonparametric data, and one-way Anova
562 with post-hoc Tukey HSD test for comparison of 3 or more groups. Box plot upper and lower
563 hinges represent the first and third quartiles, the center line indicates the median, and the
564 whiskers extends from the hinge to the highest and lowest value no further than 1.5 * (inter-
565 quartile range) from the hinge unless otherwise stated.
566
567 **Study Approval**
568 PBMCs we isolated from Trima residues from Trima Apheresis collection kits and were obtained
569 from healthy donors after written informed consent at the Blood Centers of the Pacific. Human
570 prenatal tissues (16 to 22 weeks gestational age) were obtained from terminations of pregnancy
571 after maternal written informed consent with approval from and under the guidelines of the
572 UCSF Research Protection program. Samples were excluded in the cases of known maternal
573 infection, intrauterine prenatal demise, and/or known or suspected chromosomal abnormality.
574
575 **Author Contributions**
576 VL and JH designed research studies. VL, SP, SM, and JH conducted experiments. VL, SP,
577 SM, JH acquired data. VL, SP, DB, GF, and JH analyzed data. VL and JH wrote the
578 manuscript. TB and JH provided material.
579
580 **Acknowledgements**
581 This work was supported by the UCSF Clinical and Translational Science Institute (CTSI) Pilot
582 Award for Basic and Translational Investigators (2014908), the NIAID (K08 AI128007), and the

583 Burroughs Wellcome Fund (1019828). We acknowledge the Parnassus Flow Cytometry CoLab

584 (PFCC) (RRID:*SCR_018206*) for assistance generating Flow Cytometry data. Research

585 reported here was supported in part by the DRC Center Grant NIH P30 DK063720."

586

587 **References**

588 1. Spencer J, Dillon SB, Isaacson PG, MACDONALD TT. T cell subclasses in fetal human
589 ileum. Clin Exp Immunol. 1986;65(3):553–8.

590 2. Lobach DF, Haynes BF. Ontogeny of the human thymus during fetal development. J Clin
591 Immunol. 1987 Mar;7(2):81–97.

592 3. Darrasse-Jeze G. Ontogeny of CD4+CD25+ regulatory/suppressor T cells in human fetuses.
593 Blood. 2005;105(12):4715–21.

594 4. Cupedo T, Nagasawa M, Weijer K, Blom B, Spits H. Development and activation of
595 regulatory T cells in the human fetus. Eur J Immunol. 2005 Feb;35(2):383–90.

596 5. Jain N. The early life education of the immune system: Moms, microbes and (missed)
597 opportunities. Gut Microbes. 2020 Nov 9;12(1):1824564.

598 6. Rudd BD. Neonatal T Cells: A Reinterpretation. Annu Rev Immunol. 2020 Apr 26;38(1):229–
599 47.

600 7. Zhu J, Yamane H, Paul WE. Differentiation of Effector CD4 T Cell Populations. Annu Rev
601 Immunol. 2010 Mar 1;28(1):445–89.

602 8. Kawabe T, Jankovic D, Kawabe S, Huang Y, Lee PH, Yamane H, et al. Memory-phenotype
603 $CD4^+$ T cells spontaneously generated under steady-state conditions exert innate T_H 1-like
604 effector function. Sci Immunol [Internet]. 2017 Jun 9 [cited 2022 Jun 30];2(12). Available
605 from: https://www.science.org/doi/10.1126/sciimmunol.aam9304

606 9. Min B, McHugh R, Sempowski GD, Mackall C, Foucras G, Paul WE. Neonates Support
607 Lymphopenia-Induced Proliferation. Immunity. 2003 Jan;18(1):131–40.

608 10. Smith NL, Patel RK, Reynaldi A, Grenier JK, Wang J, Watson NB, et al. Developmental
609 Origin Governs CD8+ T Cell Fate Decisions during Infection. Cell. 2018 Jun;174(1):117-
610 130.e14.

611 11. Masopust D, Vezys V, Marzo AL, Lefrançois L. Preferential Localization of Effector Memory
612 Cells in Nonlymphoid Tissue. Science. 2001 Mar 23;291(5512):2413–7.

613 12. Sathaliyawala T, Kubota M, Yudanin N, Turner D, Camp P, Thome JJC, et al. Distribution
614 and Compartmentalization of Human Circulating and Tissue-Resident Memory T Cell
615 Subsets. Immunity. 2013 Jan;38(1):187–97.

616 13. Schreurs RRCE, Baumdick ME, Sagebiel AF, Kaufmann M, Mokry M, Klarenbeek PL, et al.
617 Human Fetal TNF-α-Cytokine-Producing CD4+ Effector Memory T Cells Promote Intestinal
618 Development and Mediate Inflammation Early in Life. Immunity. 2019 Feb;50(2):462-476.e8.

619 14. Halkias J, Rackaityte E, Hillman SL, Aran D, Mendoza VF, Marshall LR, et al. CD161
620 contributes to prenatal immune suppression of IFN-γ–producing PLZF+ T cells. J Clin
621 Invest. 2019 Jul 29;129(9):3562–77.

622 15. Stras SF, Werner L, Konnikova L. Maturation of the Human Intestinal Immune System
623 Occurs Early in Fetal Development. Dev Cell. 2019;51:357–73.

624 16. Li N, van Unen V, Abdelaal T, Guo N, Kasatskaya SA, Ladell K, et al. Memory CD4+ T cells
625 are generated in the human fetal intestine. Nat Immunol. 2019 Mar;20(3):301–12.

626 17. Azizi E, Carr A, Plitas G, Rudensky A, Pe'er D. Single-Cell Map of Diverse Immune
627 Phenotypes in the Breast Tumor Microenvironment. Cell. 2018;(174):1293–308.

628 18. Szabo PA, Levitin HM, Miron M, Snyder ME, Senda T, Yuan J, et al. Single-cell
629 transcriptomics of human T cells reveals tissue and activation signatures in health and
630 disease. Nat Commun. 2019 Dec;10(1):4706.

631 19. Low JS, Farsakoglu Y, Amezcua Vesely MC, Sefik E, Kelly JB, Harman CCD, et al. Tissue-
632 resident memory T cell reactivation by diverse antigen-presenting cells imparts distinct
633 functional responses. J Exp Med. 2020 Aug 3;217(8):e20192291.

634 20. Simoni Y, Becht E, Fehlings M, Loh CY, Koo SL, Teng KWW, et al. Bystander CD8+ T cells
635 are abundant and phenotypically distinct in human tumour infiltrates. Nature. 2018
636 May;557(7706):575–9.

637 21. Alanio C, Nicoli F, Sultanik P, Flecken T, Perot B, Duffy D, et al. Bystander hyperactivation
638 of preimmune CD8+ T cells in chronic HCV patients. eLife. 2015 Nov 14;4:e07916.

639 22. Tough DF, Borrow P, Sprent J. Induction of Bystander T Cell Proliferation by Viruses and
640 Type I Interferon In Vivo. Sci New Ser. 1996;272(5270):1947–50.

641 23. Lee HG, Cho MZ, Choi JM. Bystander CD4+ T cells: crossroads between innate and
642 adaptive immunity. Exp Mol Med. 2020 Aug;52(8):1255–63.

643 24. Fry TJ, Connick E, Falloon J, Lederman MM, Liewehr DJ, Spritzler J, et al. A potential role
644 for interleukin-7 in T-cell homeostasis. 2001;97(10):8.

645 25. Kassiotis G, Zamoyska R, Stockinger B. Involvement of Avidity for Major Histocompatibility
646 Complex in Homeostasis of Naive and Memory T Cells. J Exp Med. 2003 Apr
647 21;197(8):1007–16.

648 26. Palmer MJ, Mahajan VS, Chen J, Irvine DJ, Lauffenburger DA. Signaling thresholds govern
649 heterogeneity in IL-7-receptor-mediated responses of naïve $CD8^+$ T cells. Immunol Cell
650 Biol. 2011 Jul;89(5):581–94.

651 27. Sood A, Lebel M, Dong M, Fournier M, Vobecky SJ, Haddad É, et al. CD5 levels define
652 functionally heterogeneous populations of naïve human CD4 $^{+}$ T cells. Eur J Immunol. 2021
653 Jun;51(6):1365–76.

654 28. Michaëlsson J, Mold JE, McCune JM, Nixon DF. Regulation of T Cell Responses in the
655 Developing Human Fetus. J Immunol. 2006 May 15;176(10):5741–8.

656 29. Mold JE, Michaëlsson J, Burt TD, Muench MO, Beckerman KP, Busch MP, et al. Maternal
657 Alloantigens Promote the Development of Tolerogenic Fetal Regulatory T Cells in Utero.
658 Science. 2008 Dec 5;322(5907):1562–5.

659 30. Schönland SO, Zimmer JK, Lopez-Benitez CM, Widmann T, Ramin KD, Goronzy JJ, et al.
660 Homeostatic control of T-cell generation in neonates. Blood. 2003 Aug 15;102(4):1428–34.

661 31. Barata JT, Durum SK, Seddon B. Flip the coin: IL-7 and IL-7R in health and disease. Nat
662 Immunol. 2019 Dec;20(12):1584–93.

663 32. Seddon B, Zamoyska R. TCR and IL-7 Receptor Signals Can Operate Independently or
664 Synergize to Promote Lymphopenia-Induced Expansion of Naive T Cells. J Immunol. 2002
665 Oct 1;169(7):3752–9.

666 33. Chattopadhyay PK, Yu J, Roederer M. Live-cell assay to detect antigen-specific CD4+ T-cell
667 responses by CD154 expression. Nat Protoc. 2006 Jun;1(1):1–6.

668 34. Lee YJ, Jeon YK, Kang BH, Chung DH, Park CG, Shin HY, et al. Generation of PLZF+
669 CD4+ T cells via MHC class II–dependent thymocyte–thymocyte interaction is a
670 physiological process in humans. J Exp Med. 2010 Jan 18;207(1):237–46.

671 35. Sallusto F, Lenig D, Lanzavecchia A. Two subsets of memory T lymphocytes with distinct
672 homing potentials and effector functions. Nature. 1999;401:708–12.

673 36. Surh CD, Sprent J. Homeostasis of Naive and Memory T Cells. Immunity. 2008
674 Dec;29(6):848–62.

675 37. Bains I, Antia R, Callard R, Yates AJ. Quantifying the development of the peripheral naive
676 CD4+ T-cell pool in humans. 2009;113(22):5480–7.

677 38. den Braber I, Mugwagwa T, Vrisekoop N, Westera L, Mögling R, Bregje de Boer A, et al.
678 Maintenance of Peripheral Naive T Cells Is Sustained by Thymus Output in Mice but Not
679 Humans. Immunity. 2012 Feb;36(2):288–97.

680 39. Tan JT, Dudl E, LeRoy E, Murray R, Sprent J, Weinberg KI, et al. IL-7 is critical for
681 homeostatic proliferation and survival of naïve T cells. Proc Natl Acad Sci. 2001 Jul
682 17;98(15):8732–7.

683 40. Younes SA, Punkosdy G, Caucheteux S, Chen T, Grossman Z, Paul WE. Memory
684 Phenotype CD4 T Cells Undergoing Rapid, Nonburst-Like, Cytokine-Driven Proliferation
685 Can Be Distinguished from Antigen-Experienced Memory Cells. Marrack P, editor. PLoS
686 Biol. 2011 Oct 11;9(10):e1001171.

687 41. Huang HY, Luther SA. Expression and function of interleukin-7 in secondary and tertiary
688 lymphoid organs. Semin Immunol. 2012 Jun;24(3):175–89.

689 42. Rackaityte E, Halkias J, Fukui EM, Mendoza VF, Hayzelden C, Crawford ED, et al. Viable
690 bacterial colonization is highly limited in the human intestine in utero. Nat Med. 2020
691 Apr;26(4):599–607.

692 43. Mishra A, Lai GC, Yao LJ, Aung TT, Shental N, Rotter-Maskowitz A, et al. Microbial
693 exposure during early human development primes fetal immune cells. Cell. 2021
694 Jun;184(13):3394–409.

695 44. Seddon B, Legname G, Tomlinson P, Zamoyska R. Long-Term Survival but Impaired
696 Homeostatic Proliferation of Naïve T Cells in the Absence of p56lck. Sci New Ser.
697 2000;290(5489):127–31.

698 45. Kawabe T, Yi J, Kawajiri A, Hilligan K, Fang D, Ishii N, et al. Requirements for the
699 differentiation of innate T-bet high memory-phenotype CD4+ T lymphocytes under steady
700 state. Nat Commun. 2020 Dec;11(1):3366.

701 46. Hirota K, Turner JE, Villa M, Duarte JH, Demengeot J, Steinmetz OM, et al. Plasticity of
702 TH17 cells in Peyer's patches is responsible for the induction of T cell–dependent IgA
703 responses. Nat Immunol. 2013 Apr;14(4):372–9.

704 47. Ivanov II, McKenzie BS, Zhou L, Tadokoro CE, Lepelley A, Lafaille JJ, et al. The Orphan
705 Nuclear Receptor RORγt Directs the Differentiation Program of Proinflammatory IL-17+ T
706 Helper Cells. Cell. 2006 Sep;126(6):1121–33.

707 48. Stockinger B, Omenetti S. The dichotomous nature of T helper 17 cells. Nat Rev Immunol.
708 2017 Sep;17(9):535–44.

709 49. McGovern N, Shin A, Low G, Low D, Duan K, Yao LJ, et al. Human fetal dendritic cells
710 promote prenatal T-cell immune suppression through arginase-2. Nature. 2017
711 Jun;546(7660):662–6.

712 50. May K, Grube M, Malhotra I, Long CA, Singh S, Mandaliya K, et al. Antibody-Dependent
713 Transplacental Transfer of Malaria Blood-Stage Antigen Using a Human Ex Vivo Placental
714 Perfusion Model. PLoS ONE. 2009 Nov 24;4(11):e7986.

715 51. Halkias J, Melichar HJ, Taylor KT, Ross JO, Yen B, Cooper SB, et al. Opposing chemokine
716 gradients control human thymocyte migration in situ. J Clin Invest. 2013 May
717 1;123(5):2131–42.

718 52. Dobin A, Davis CA, Schlesinger F, Drenkow J, Zaleski C, Jha S, et al. STAR: ultrafast
719 universal RNA-seq aligner. Bioinformatics. 2013 Jan;29(1):15–21.

720 53. Anders S, Huber W. Differential expression analysis for sequence count data. Genome Biol.
721 2010;R106.

722 54. Finak G, McDavid A, Yajima M, Deng J, Gersuk V, Shalek AK, et al. MAST: a flexible
723 statistical framework for assessing transcriptional changes and characterizing heterogeneity
724 in single-cell RNA sequencing data. Genome Biol. 2015 Dec;16(1):278.

55. Bunis DG, Andrews J, Fragiadakis GK, Burt TD, Sirota M. dittoSeq: universal user-friendly single-cell and bulk RNA sequencing visualization toolkit. Alfonso V, editor. Bioinformatics. 2021 Apr 1;36(22–23):5535–6.

56. Zhou Y, Zhou B, Pache L, Chang M, Khodabakhshi AH, Tanaseichuk O, et al. Metascape provides a biologist-oriented resource for the analysis of systems-level datasets. Nat Commun. 2019 Dec;10(1):1523.

Figures

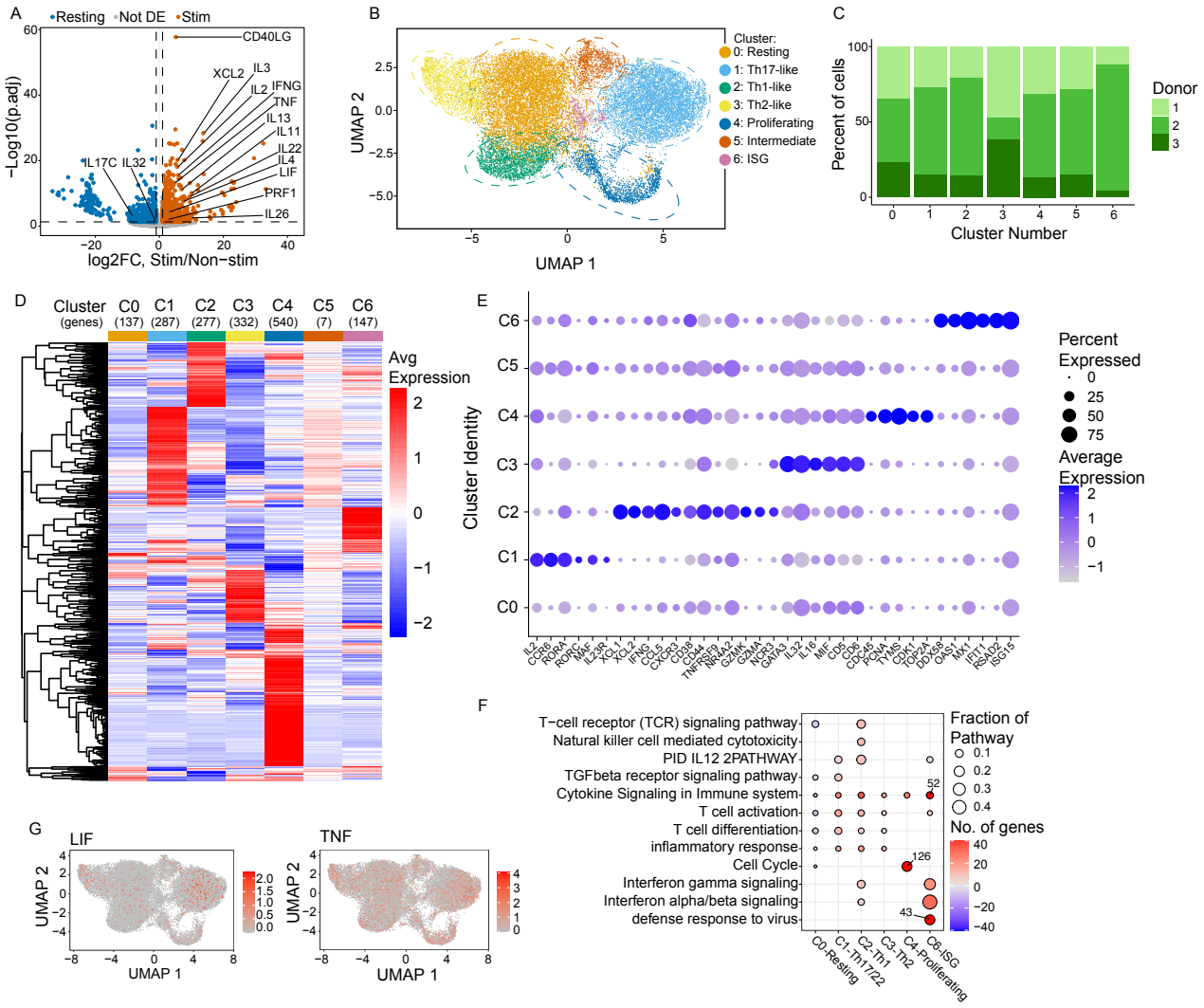

Figure 1. Prenatal PLZF⁺ CD4⁺ T cells in the small intestine are a heterogeneous population.
(A) Volcano plot of differentially expressed (DE) genes (log2 fold change > 1, FDR ≤ 0.05) from bulk RNA-seq in stimulated (PMA/ionomycin) versus unstimulated small intestine (SI) PLZF⁺ CD4⁺ T cells identifies enriched (orange) versus diminished (blue) transcripts in stimulated cells. Select cytokines are labeled. (B) UMAP plot of unsupervised (Louvain) clustering of scRNA-seq transcriptional profile of 23,676 sort-purified, PLZF⁺ Vα7.2⁻ CD4⁺ TCRαβ⁺ T cells from the SI of 3 donors, each cluster surrounded by a median centered ellipse and (C) the proportion of cells from each donor in each cluster. (D) Heat map of unsupervised hierarchical clustering of DE genes and (E) dot plot of selected DE genes within each identified cluster of PLZF⁺CD4⁺ T cells. (F) Selected GO terms, Reactome Gene Sets, and KEGG pathways from Metascape analysis of cluster-specific DE gene lists. Downregulated pathways are indicated with negative number of genes and outliers indicated with text overlay. G) UMAP plots of *LIF* and *TNF* expression among SI PLZF⁺CD4⁺ T cells.

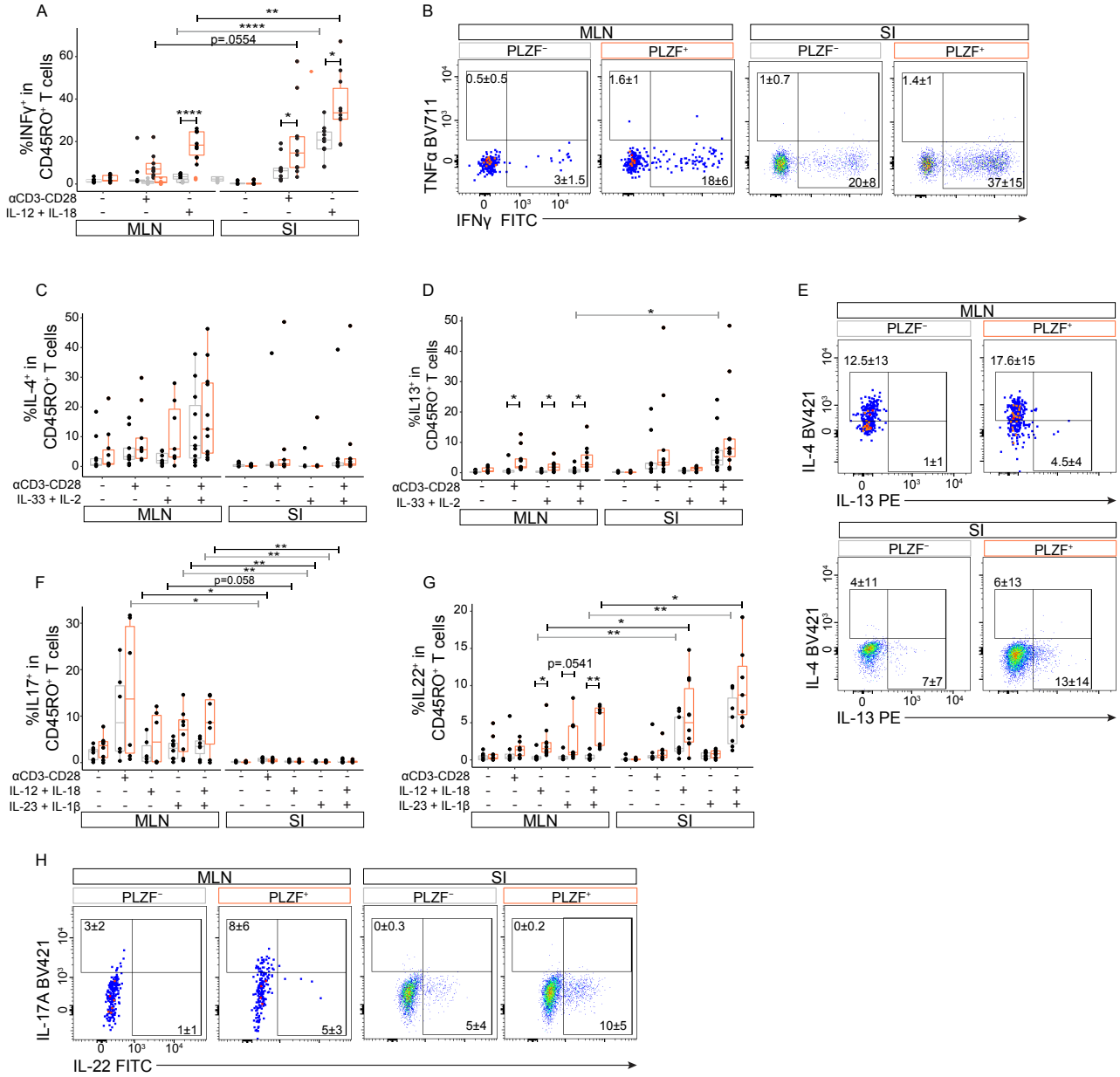

Figure 2: Prenatal PLZF⁺ CD4⁺ T cells display spatially compartmentalized effector function.

Quantification (A, C, D, F, G) and representative flow plots (B, E, H) of indicated intracellular cytokine staining after stimulation among PLZF⁻ (grey) and PLZF⁺(orange) CD45RO⁺ CD4⁺ T cells isolated from the small intestine (SI) and mesenteric lymph node (MLN). Cells were stimulated as indicated for 16 hours, and Brefeldin A added in the last 4 hours. Flow plots indicate intracellular cytokine staining following stimulation with IL-12 + IL-18 (B), αCD3/CD28 monoclonal antibodies (mAbs) + IL-33 + IL-2 (D), and IL-23 + IL-1β + IL-12 + IL-18 (H). Circles represent individual donors. Paired ANOVA with Tukey multiple comparison test (A, C, D, F, G) *p < 0.05, **p < 0.01, ***p<0.001 ****p < 0.0001. Large dots used for improved visualization of small cell numbers. Numbers in flow cytometry plots represent means of frequencies of gated populations ± SD.

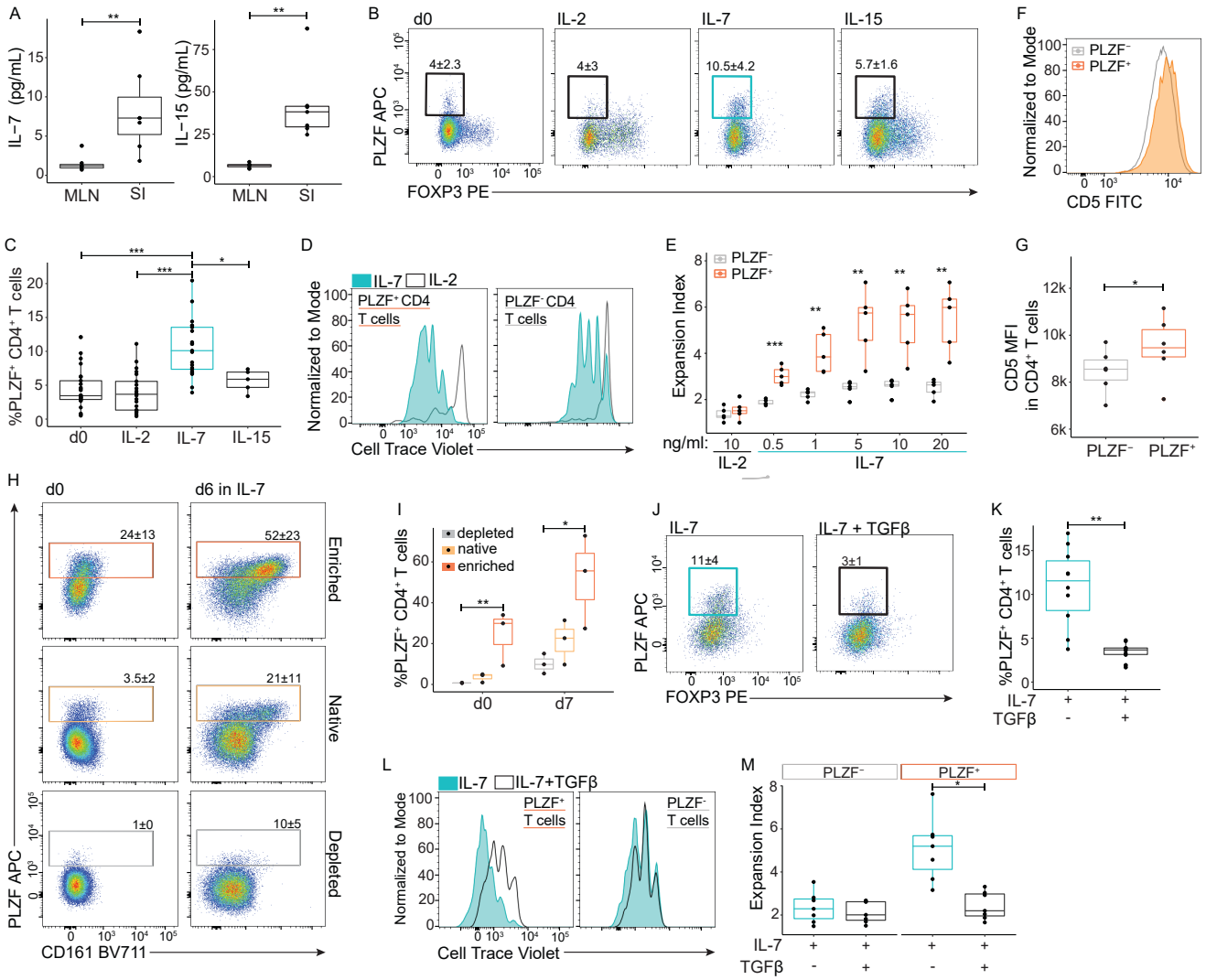

Figure 3. IL-7 and TGFb reciprocally regulate the expansion of prenatal PLZF⁺ CD4⁺ naïve T cells.

(A) Quantification of whole tissue concentrations of IL-7 and IL-15 measured by cytokine bead array. (B) Representative flow cytometry plots and (C) frequencies of PLZF⁺ CD4⁺ T cells derived from naïve CD4⁺ T cells before initiation of culture (d0) and after 6 days of culture with IL-2, IL-7, or IL-15 (10ng/mL). (D) Representative histograms of Cell Trace Violet (CTV) dilution, and (E) expansion indices of PLZF⁺ and PLZF⁻ CD4⁺ T cells cultured for 6 days as indicated. (F) Representative histogram and (G) MFI of CD5 expression on PLZF⁺- or PLZF⁻-naïve CD4⁺ T cells. (H) Representative post-sort flow plots and (I) quantification of naïve PLZF⁺ CD4⁺ T cells before initiation of culture (d0) and after 6 days of culture with 10ng/mL IL-7. (J) Representative flow plots and (K) proportion of PLZF⁺ CD4⁺ T cells after 6 days of culture with IL-7 +/- TGFb. (L) Representative histograms of CTV dilution and (M) expansion indices of PLZF⁺ and PLZF⁻ CD4⁺ T cells cultured for 6 days in the presence of IL-7 +/- TGFb (10ng/mL). Circles represent individual donors. Wilcoxon Signed Rank Test (A, G, K, M) and Paired ANOVA with Tukey's multiple comparison test (C, E, I) *p < 0.05, **p < 0.01, ***p<0.001 ****p < 0.0001. Numbers in flow cytometry plots represent means of frequencies of gated populations ± SD.

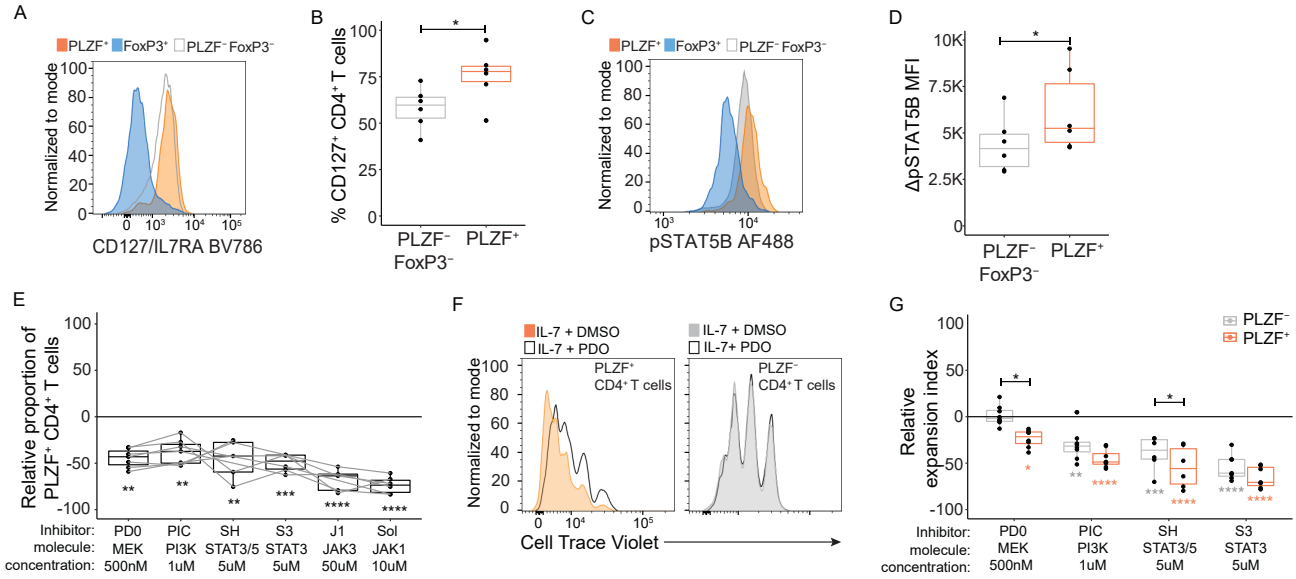

Figure 4. Differences in IL7 signaling contribute to the preferential expansion of PLZF⁺ CD4⁺ T cells.

(A) Representative histograms and (B) frequencies of IL7R expression within indicated populations of naïve CD4⁺ T cells. (C) Representative histograms and (D) Normalized MFI of phosphorylated STAT5B (pSTAT5B) among subsets of naïve CD4⁺ T cells after 30 minutes of stimulation with IL-7. (E) Relative proportions of PLZF⁺ CD4⁺ T cells normalized to DMSO control after 6-days of stimulation with IL-7 in the presence of indicated signaling inhibitors. Inhibitors used: PD0 (PD0325901, MEK), PIC (Pictilisib, PI3Kα/δ), SH (SH-4-54, STAT3 and STAT5), S3 (STAT3-IN-1, STAT3), J1 (JANEX-1, JAK3), Sol (Solcitinib, JAK1). (F) Representative histograms of CTV dilution after treatment of naïve CD4⁺ T cells with IL-7 and PD0, and (G) relative increase or decrease in expansion indices among indicated subsets of CD4⁺ T cells after 6 days of stimulation with IL-7 in the presence of indicated signaling inhibitors relative to IL-7 + DMSO control. Circles represent individual donors. Wilcoxon Signed Rank Test (B, D) and Paired ANOVA with Tukey's multiple comparison test (C, E) *$p < 0.05$, **$p < 0.01$, ***$p<0.001$ ****$p < 0.0001$. Numbers in flow cytometry plots represent means of frequencies of gated populations ± SD.

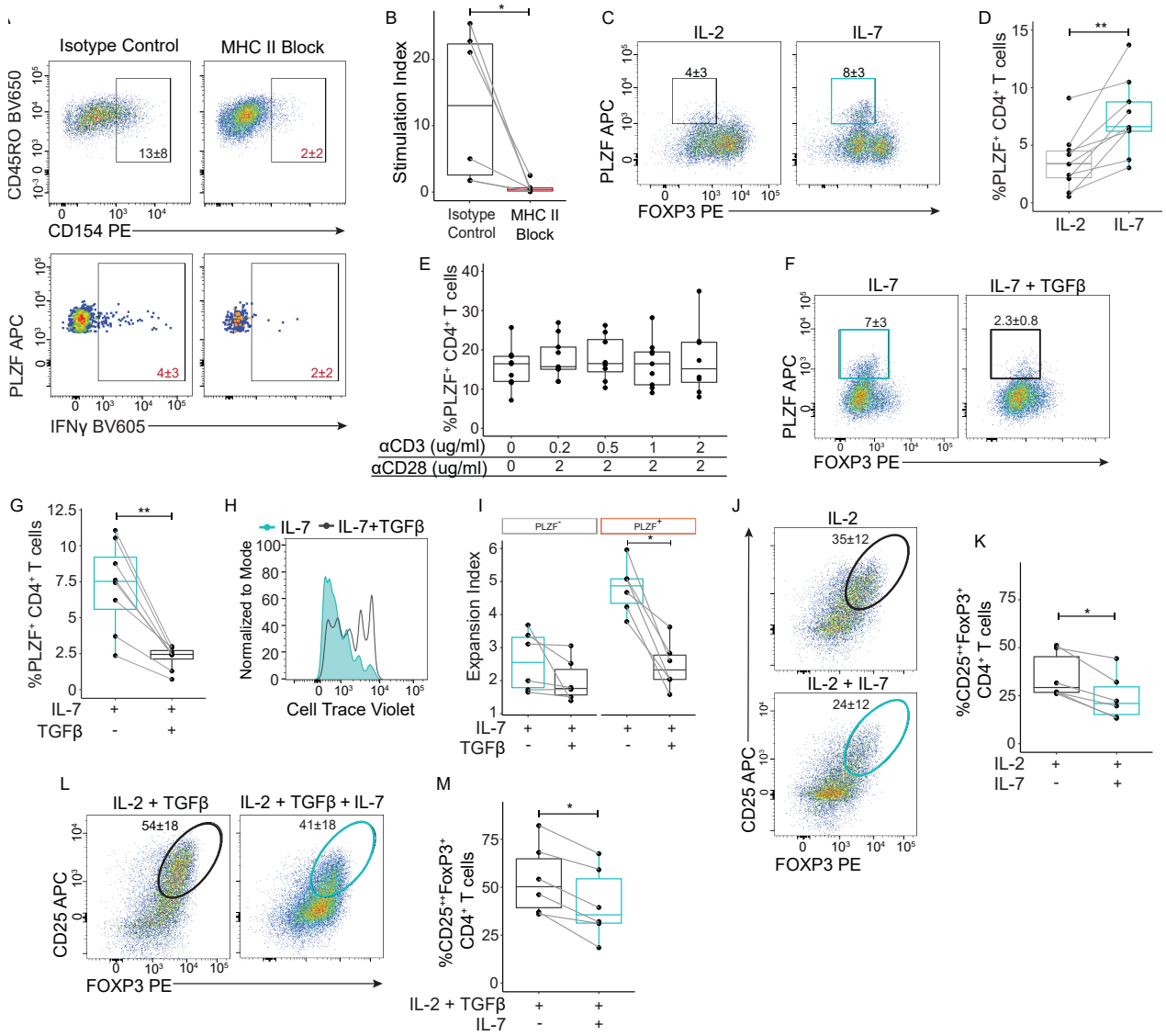

Figure 5. IL-7 and TGFβ sustain reciprocal regulation of MHC Class II restricted PLZF$^+$ CD4$^+$ naïve T cells in the presence of TCR signaling.
(A) Representative flow plots of intracellular CD40L/CD154 expression among SI PLZF$^+$CD4$^+$ T cells (top) and IFNγ production among CD154$^+$PLZF$^+$CD4$^+$ T cells (bottom) co-cultured with allogeneic adult CD14$^+$ antigen presenting cells in the presence of a pan MHC-II blocking antibody (αHLA DR-DP-DQ) or isotype control. (B) Stimulation index, calculated as the percent of CD154$^+$ IFNγ$^+$ within PLZF$^+$ T cells population after 16 hours of co-culture with enriched allogeneic adult CD14$^+$ antigen presenting cells in the presence of a pan MHC II blocking antibody (αHLA DR-DP-DQ) or isotype control (IgG$_2$). (C) Representative flow plots and (D) frequencies of PLZF$^+$ CD4$^+$ T cells derived from naïve CD4$^+$ T cells stimulated with αCD3/CD28 in the presence of IL-2 or IL-7 for 6 days. (E) Proportions of PLZF$^+$-CD4$^+$ T cells stimulated with indicated concentrations of αCD3/CD28 in the presence of IL-7 for 12 days. (F) Representative flow plots and (G) proportions of PLZF$^+$ CD4$^+$ T cells after 6 days of stimulation with αCD3/CD28 in the presence of IL-7 +/- TGFβ. (H) Representative histograms of CTV dilution,

836 and (I) Expansion indices of PLZF$^+$ among indicated CD4$^+$T cells after 6 days of stimulation with
837 αCD3/CD28 in the presence of IL-7 +/- TGFβ. (J, L) Representative flow plots and (K, M)
838 frequencies of CD25^{hi} FoxP3$^+$ CD4$^+$ T cells after 6 days of αCD3/CD28 stimulation in the
839 presence of indicated cytokines. Circles represent individual donors. Wilcoxon Signed Rank
840 Test (B, D, I, K, M) and Paired ANOVA with Tukey's multiple comparison test (E) *p < 0.05, **p
841 < 0.01, ***p<0.001 ****p < 0.0001. Numbers in flow cytometry plots represent means of
842 frequencies of gated populations ± SD.

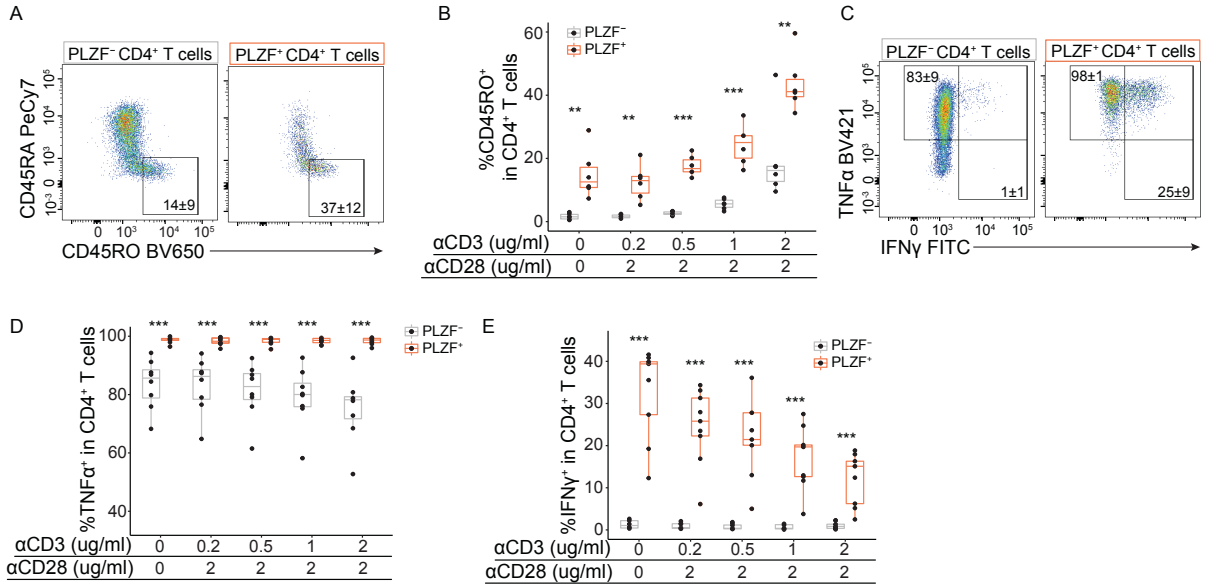

843

844 **Figure 6. IL-7 alone promotes memory phenotype acquisition in PLZF$^+$CD4$^+$ T cells.**
845 (A) Representative flow plots and (B) frequencies of CD45RO$^+$ cells among PLZF$^+$ and PLZF$^-$
846 CD4$^+$T cells after 12 days of culture with IL-7 and indicated αCD3/CD28 concentrations. (C)
847 Representative flow plots of intracellular cytokine staining and (D, E) frequencies of (D) TNFα$^+$
848 cells and (E) IFNγ$^+$ cells among CD4$^+$T cells after 12 days of culture with IL-7 and indicated
849 αCD3/CD28 concentrations and following re-stimulation with PMA/ionomycin. Circles represent
850 individual donors. Paired ANOVA with Tukey's multiple comparison test (B, D, E) *p < 0.05, **p
851 < 0.01, ***p<0.001 ****p < 0.0001. Numbers in flow cytometry plots represent mean frequency ±
852 SD of gated populations.
853

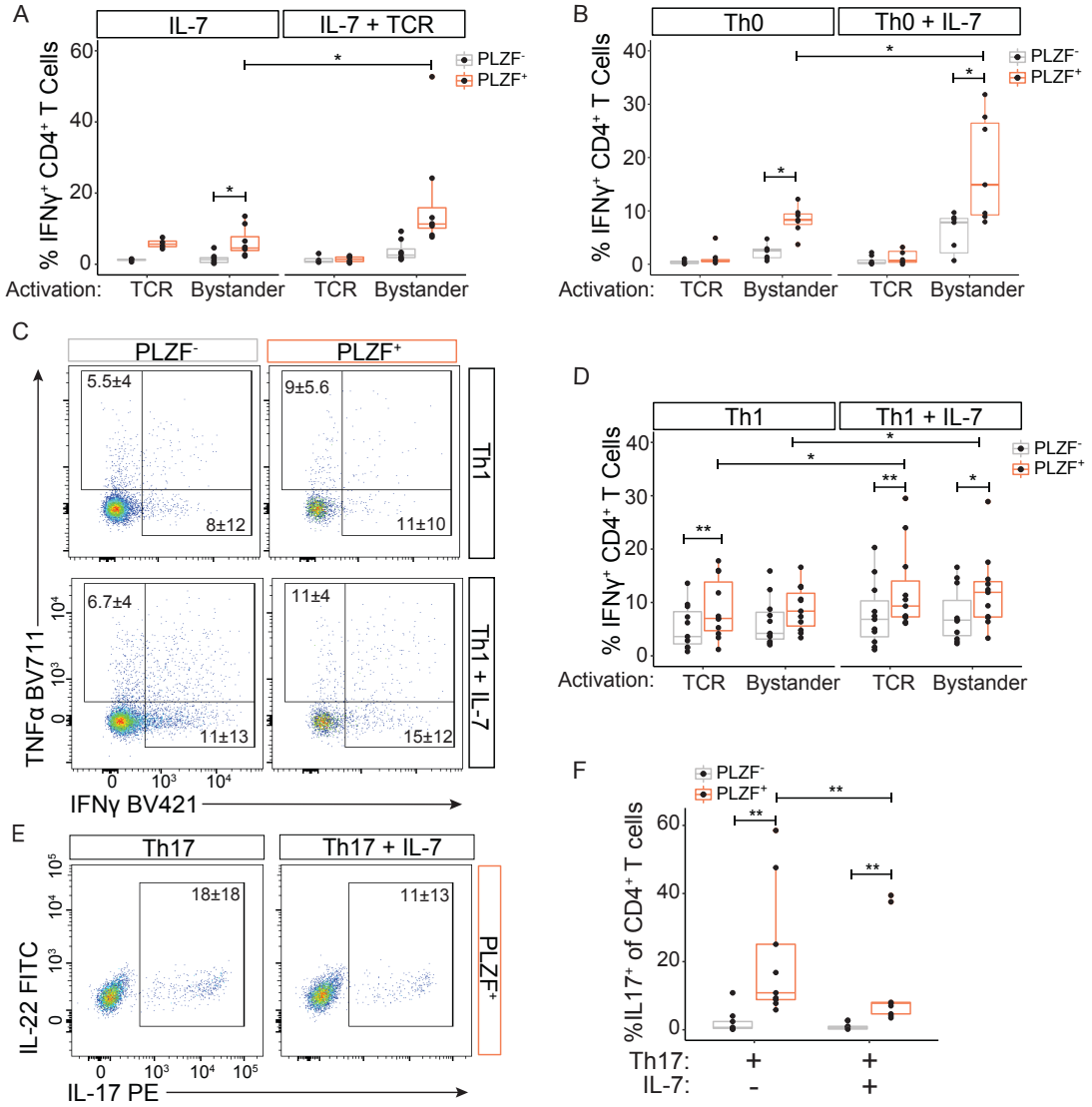

Figure 7. IL-7 modulates the effector maturation of prenatal PLZF$^+$ CD4$^+$ T cells. Functional studies following a two-step in vitro culture in which naïve CD4$^+$ T cells were first expanded in the presence of IL-7 alone, followed by 7 days of maturation in the indicated conditions: IL-7 alone, IL-7 + TCR (stimulated with αCD3/CD28 mAbs), Th0 (TCR + IL-2); Th1 (TCR + IL-12), Th17 (TCR + IL-23 + IL-1β) (A, B, D) Proportions of IFNγ$^+$ cells among CD4$^+$ T cell subsets matured in the indicated conditions and following 24 hour re-stimulation with αCD3/CD28 (TCR) or IL-12/IL-18 (Bystander). (C) Representative flow plots of intracellular cytokine staining among CD4$^+$ T cells differentiated under indicated conditions following re-stimulation with αCD3/CD28. E) Representative flow plots of intracellular cytokine staining and F) proportions of IL-17$^+$ cells among indicated CD4$^+$ T cells matured under Th17-skewing conditions +/- IL7 and following PMA/ionomycin stimulation. Circles represent individual donors. Wilcoxon Signed Rank Test to compare PLZF$^+$ to PLZF$^-$ fractions and paired stimulations across maturation conditions (A, B, D, F). Numbers in flow cytometry plots represent means of frequencies of gated populations ± SD.